Elastic and inelastic scattering of ^{58}Ni + ^{90,94}Zr

Y. Sugiyama[1], D.R. Napoli[2], A.M. Stefanini[2], L. Corradi[2], C. Signorini[3], F. Scarlassara[3], Y. Tomita[1], H. Ikezoe[1], K. Ideno[1], Y. Yamanouchi[1], Y. Nagashima[4], T. Sugimitsu[5], G. Pollarolo[6]

[1] Advanced Science Research Center, JAERI, Tokai-mura,Ibaraki-ken 319-1195, Japan
[2] INFN Laboratori Nazionali di Legnaro, via Romea 4, I-35020 Legnaro (Pd), Italy
[3] Dipartimento di Fisica dell'Universitá di Padova and INFN Sezione di Padova, Padova, Italy
[4] College of Medical Technology and Nursing, Tsukuba, Ibaraki-ken 305, Japan
[5] Depatment of Physics, University of Kyushu, Fukuoka 812, Japan
[6] Dipartimento di Fisica Teorica dell'Universitá di Torino and INFN Sezione di Torino, via P. Giuria 1, I-10125 Torino, Italy

Abstract. Pure elastic and inelastic scattering cross sections have been measured for the systems ^{58}Ni + ^{90,94}Zr at energies near the Coulomb barrier where not only quasi-elastic and fusion but also deep-inelastic process come into play. Coupled channels calculations including both projectile and target inelastic excitations can successfully explain the elastic and inelastic scattering angular distributions with an energy-independent semi-empirical bare potential. The calculation reproduces also the sum of the total quasi-elastic, fusion and deep-inelastic cross sections.

PACS. 25.70.Bc Elastic and quasielastic scattering

1 Introduction

It is known that couplings between reaction channels become prominent at energies around the Coulomb barrier in heavy-ion induced reactions [1,2]. Large enhancements of subbarrier fusion cross section and the so called threshold anomaly in elastic scattering are typical consequences of the coupling effects. The coupled-channels(CC) approach to heavy-ion collisions provides therefore a consistent framework for simultaneously calculating elastic and inelastic scattering, transfer reactions and fusion cross sections. The essential inputs required for the CC calculations are the energy-independent ion-ion potential for describing elastic scattering and the couplings which cause transitions into dominant reaction channels. Then the energy-dependent polarization potential is generated implicitly from the couplings. This approach has an advantage that it can display explicitly the interplay between various couplings, and it allows one to incorporate directly nuclear information which may be available from independent sources. Successful results has been obtained for e.g. the ^{28}Si+ ^{58,64}Ni systems where quasi-elastic scattering [3] and the fusion cross sections [4] have been measured at energies near the Coulomb barrier. The CC calculations including inelastic excitations and neutron transfers have explained well the energy dependence of the quasi-elastic scattering and fusion cross sections with a single energy-independent bare potential [3].

Systematic measurements of pure elastic scattering up to heavier systems are indispensable for obtaining a unified description of ion-ion potentials. However pure elastic scattering date are scarce especially in medium heavy systems, since measurement of pure elastic scattering becomes very difficult because of the severe limit one has on the energy resolution. At the same time CC calculations become more complicated in medium heavy systems because the number of open channels increases and complicated processes like e.g. deep inelastic scattering come into play at energies around the Coulomb barrier. It is not practical to take into account all of the open channels. Instead it is important to know the most dominant reaction channels which determine the energy-dependent polarization potential. This leads to obtaining the energy-independent bare potential whose imaginary part is interpreted as describing the depopulation of the entrance channel due to the channels not included explicitly in the calculations.

We present in this work an accurate measurement of the ^{58}Ni + ^{90,94}Zr pure elastic and inelastic scattering cross sections to the low lying levels, at Nickel energies of E$_{lab}$ = 230.2 and 245 MeV. In a previous experiment [5] at the same energies not only fusion evaporation residue and transfer cross sections but also deep-inelastic scattering with large cross sections were measured. It is important to study how the elastic scattering is described in the presence of a strong deep-inelastic process.
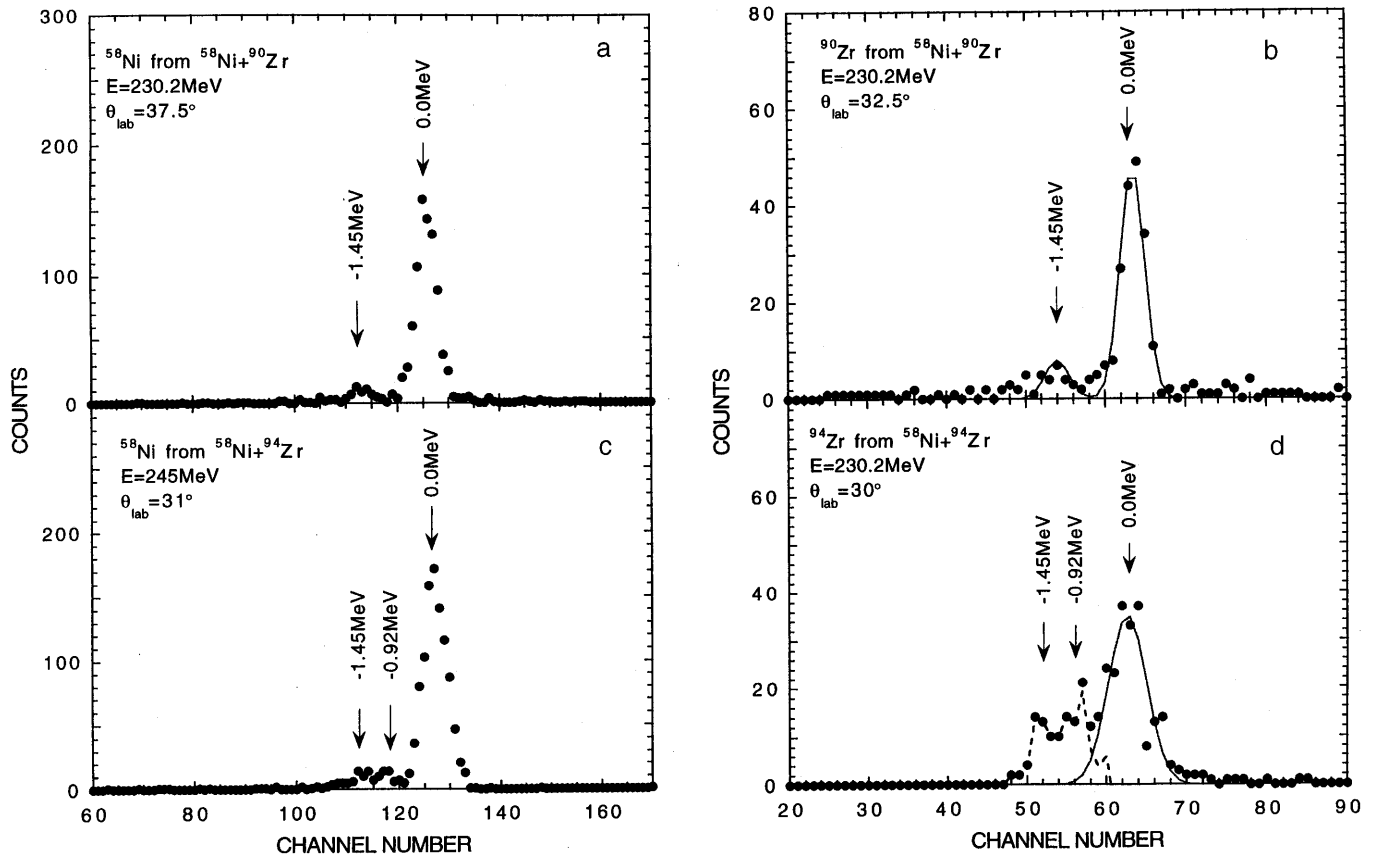
Fig. 1. Position (momentum) spectra from the ^{58}Ni+^{90}Zr reaction at $E_{lab} = 230.2$ MeV, **a** for ^{58}Ni at $\theta_{lab} = 37.5^o$, **b** for ^{90}Zr at $\theta_{lab} = 32.5^o$, **c** position spectra from the ^{58}Ni + ^{94}Zr reaction are shown for ^{58}Ni at $E_{lab} = 245.0$ MeV and at $\theta_{lab} = 31^o$, **d** for ^{94}Zr at $E_{lab} = 230.2$ MeV and at $\theta_{lab} = 30^o$. The solid line in **d** is a gaussian fit to the elastic peak. The bulk of low-lying inelastic excitations was obtained by subtracting the gaussian from the data. Q-values of elastic and inelastic peaks are indicated with arrows

2 Experiment and results

The measurements of pure elastic scattering are not an easy task for heavy systems where one needs good mass, nuclear charge and energy resolutions with a good statistic as well as very thin and homogeneous target to avoid strong energy spreads. In addition, large kinematic momentum shifts k complicate the situation. Conventional time-of-flight systems have limited energy resolutions; kinematic coincidence setups also do not always meet the requirements necessary to separate the elastic events from the inelastic excitations of the lowest levels. In the present experiment, the lowest excited states are situated at 1.45 MeV for the 2^+ of ^{58}Ni and at 0.92 MeV (1.76 MeV) for the 2^+ of ^{94}Zr (^{90}Zr). To solve this point we have used the heavy-ion magnetic spectrograph ENMA [6] at JAERI. It has a characteristic feature that the kinematic momentum shift is well compensated, so that a high energy resolution is achieved over a wide range of k. A detailed description of the features and performance of ENMA can be found in [6].

The ^{58}Ni beam with typical intensities of 10 pnA was obtained from the JAERI tandem accelerator at ener-

gies of 230.2 and 245.0 MeV. These energies were chosen to match the existing data on fusion, deep-inelastic and transfer reactions of Scarlassara et al. [5] and are already corrected for the target thickness. We used targets of ^{90,94}Zr of 10μg/cm^2 evaporated on 10μg/cm^2 carbon backing. The target enrichments were 97.65% and 91.2% for ^{90,94}Zr, respectively. Proper normalization between the different runs was insured by two monitor detectors placed at forward angles. The outgoing particles were momentum analyzed in the magnetic spectrograph ENMA and detected in the focal plane with a 40cm long hybrid focal plane detector [7]. Its entrance slits define the maximum integration angle for the angular distribution $\Delta\theta_{lab} = \pm 1.65^o$ (horizontal plane) and $\Delta\phi_{lab} = \pm 1^o$ (vertical plane) which correspond to a solid angle of 1.44 msr. The combined effect of the magnetic elements effectively corrects for the kinematic energy spreads which typically are $\approx$ 2-3 MeV/deg. From a measurement of total energy E, energy loss (δE) and position (Bρ) we could identify Ni and Zr particles. The data at backward angles ($\theta_{cm} \geq 90^o$) were obtained by detecting the forward recoiling Zr ions. In Fig. 1 momentum spectra of ^{58}Ni and ^{90,94}Zr from the ^{58}Ni + ^{90,94}Zr reactions are shown. Q-values of elastic and
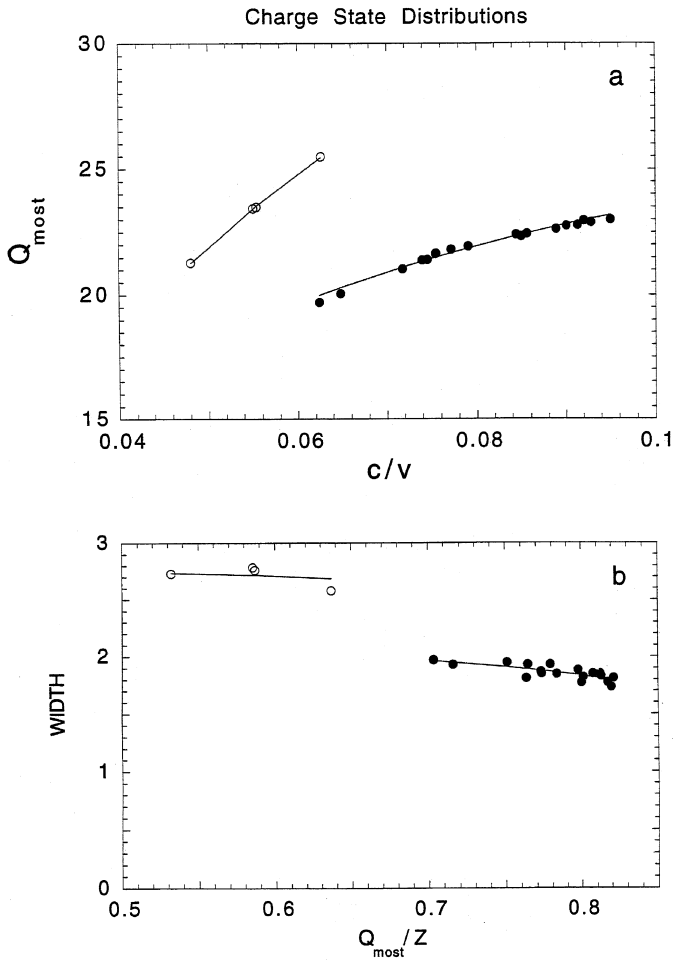
Fig. 2. The most probable charge state, q_m, and the width, w_q, of the charge state distributions for Ni (filled circles) and Zr (open circles) isotopes as **a** functions of v/c, **b** q_m/Z (see text). Solid curves are the results obtained by the semi-empirical formula

inelastic peaks are indicated with arrows in the figures. A combined analysis of E, δE and focal plane position allows to separate out the charged particle transfer for Ni but not for Zr; on the other hand, it is also known [5] that such channels have rather small transfer cross sections at backward angles. For the Ni outgoing particles an energy resolution of about 700 keV was obtained, which was enough to have a clear separation between the elastic peak and the low-lying inelastic excitations. For the recoiling Zr particles the resolution of about 1 MeV was not enough for the clear separation berween elastic and inelastic peaks in the ^{94}Zr nucleus. We made then a gaussian fit to extract a pure elastic scattering peak that is shown by the solid line in the spectrum of the ^{58}Ni + ^{94}Zr system. The bulk of low-lying inelastic excitations up to ≃2 MeV was obtained by subtracting the gaussian from the data as shown in the figure.

Charge state distributions of outgoing Ni and Zr products were measured at several angles for each target. These were fitted with a gaussian. The obtained peaks

and widths are shown in Fig. 2 as functions of v/c and q_m/Z, where v is the ion velocity; c, the speed of light in vacuum; q_m, the most probable charge state and Z, the ion atomic number. Filled and open circles correspond to Ni and Zr data, respectively. It should be stressed that the charge state distribution was obtained in the target configuration where the outgoing Ni and Zr products passed through the carbon backing. In this way, the charge state distribution of the outgoing particle depends only on its velocity and atomic number. The target angle has been maintained as perpendicular as possible to the ENMA entrance. We have used this data to obtain the adjustable parameters of the Sayer's semi-empirical formula [8] to interpolate the charge state distribution for the other ion velocities. The semi-empirical formula predicts the most probable charge state (q_m) and the width (w_q) of the charge state distribution in a carbon foil as

$$q_m/Z = 1 - A_1 \exp[A_2 Z^{-0.38}(v/c)^{A_3}]$$

and

$$w_q = A_4 Z^{0.45}[q_m/Z(1 - q_m/Z)]^{A_5}$$

where $A_1...A_5$ are adjustable parameters. The fitted curves are shown in Fig. 2 by solid lines. The maximum errors of the cross sections due to the charge state distributions are estimated as 5%.

The angular distributions for elastic and inelastic scattering at the indicated energies are shown in Table 1 and Fig. 3 for the ^{90}Zr case and in Table 2 and Fig. 4 for the ^{94}Zr. With the energy resolution of our apparatus we have been able to extract good elastic scattering angular distribution for both ^{90}Zr and ^{94}Zr while inelastic scattering has been extracted only for the lowest 2^+ states of ^{58}Ni and ^{90}Zr in the case of ^{90}Zr. For the ^{94}Zr target the inelastic angular distributions include all the states with excitation energies up to ≃2 MeV. The errors shown in Tables 1 and 2 include statistics, monitor normalization, beam alignment, fit to the momentum spectra and charge state distributions.

Total inelastic scattering cross sections were obtained by integration of the measured angular distributions of Figs. 3 and 4. The data outside the measured angle range were extrapolated from the fitted curves by the CC calculations (see next section). The cross section to other states is negligibly small, as seen in Fig. 1. The errors quoted come from the difference between extreme extrapolations in addition to the ones listed in Tables 1 and 2. The results are listed in Table 3.

3 Analysis

An empirical ion-ion potential at large distances , which governs elastic scattering and surface reactions of heavy ions, has been derived in terms of the folding potential by Broglia and Winther [9]. A Wood-Saxon parametrization, which is adjusted to fit the tail of the empirical potential, have been successfully used in CC analyses of elastic and

Table 1. Elastic and inelastic scattering cross sections for **a** ^{58}Ni + ^{90}Zr at $E_{lab} = 230.2$ MeV, **b** at $E_{lab} = 245.0$ MeV

a

θ_{cm}	$\sigma_{el}(\theta)/\sigma_R$	$\Delta\big(\sigma_{el}(\theta)/\sigma_R\big)$	$d\sigma_{in}/d\Omega$ (mb/sr)	$\Delta\big(d\sigma_{in}/d\Omega\big)$ (mb/sr)
13.2	1.00	0.003		
29.5	0.99	0.01		
40.8	0.97	0.05		
44.8	0.98	0.01	93.	9.
48.8	0.95	0.01	98.	10.
50.4	0.92	0.04		
52.8	0.95	0.02	83.	12.
56.7	0.95	0.03	94.	15.
59.8	0.87	0.04		
60.6	0.85	0.02	93.	11.
64.5	0.83	0.03	96.	13.
67.5	0.88	0.03	89.	26.
68.3	0.91	0.04	76.	10.
72.1	0.85	0.04		
75.1	0.79	0.04		
75.9	0.81	0.05	46.	10.
78.1	0.77	0.04		
82.0	0.88	0.04		
90.0	0.76	0.05	52.	8.
100.0	0.82	0.06	44.	7.
105.0	0.65	0.04	30.	4.
106.0	0.67	0.02	22.	15.
110.0	0.63	0.05	22.	4.
115.0	0.49	0.03	15.	2.
120.0	0.29	0.02	18.	1.
125.0	0.19	0.01	15.	1.
130.0	0.11	0.007	7.6	0.7

b

θ_{CM}	$\sigma_{el}(\theta)/\sigma_R$	$\Delta\big(\sigma_{el}(\theta)/\sigma_R\big)$	$d\sigma_{in}/d\Omega$ (mb/sr)	$\Delta\big(d\sigma_{in}/d\Omega\big)$ (mb/sr)
13.2	1.00	0.02		
19.7	0.96	0.02		
29.5	1.01	0.03		
40.8	1.04	0.03	192.	27.
50.4	0.89	0.03	136.	16.
59.8	0.87	0.03	132.	11.
64.5	0.86	0.06		
67.5	0.85	0.03	108.	8.
72.1	0.85	0.03	80.	7.
75.1	0.84	0.03	88.	6.
78.1	0.84	0.03	80.	6.
82.0	0.81	0.04	81.	8.
86.0	0.86	0.04	67.	12.
90.0	0.83	0.05	43.	8.
95.0	0.63	0.05	35.	4.
100.0	0.33	0.03	22.	3.
106.0	0.11	0.01	19.	14.
109.0	0.08	0.08		
115.0	0.003	0.003		

Table 2. Elastic and inelastic scattering cross sections for ^{58}Ni + ^{94}Zr at **a** $E_{lab} = 230.2$ MeV, **b** at $E_{lab} = 245.0$ MeV. The inelastic cross sections get contributions from all the states up to an excitation energy of 2 MeV

a

θ_{CM}	$\sigma_{el}(\theta)/$ σ_{Ruth}	$\Delta\big(\sigma_{el}(\theta)/\sigma_{Ruth}\big)$	$d\sigma_{in}/d\Omega$ (mb/sr)	$\Delta\big(d\sigma_{in}/d\Omega\big)$ (mb/sr)
12.9	1.00	0.02		
19.4	1.00	0.03		
29.0	1.00	0.03	212.	30.
40.1	0.87	0.03	209.	28.
49.5	0.89	0.03	185.	20.
58.8	0.91	0.03	144.	16.
66.4	0.77	0.03	112.	9.
72.3	0.78	0.04	143.	13.
76.8	0.85	0.06	114.	16.
82.0	0.83	0.08	66.	35.
90.0	0.79	0.05	77.	25.
96.0	0.76	0.04	76.	15.
102.0	0.63	0.04	44.	12.
108.0	0.35	0.03	51.	6.
114.0	0.19	0.03	34.	7.
120.0	0.11	0.01	23.	3.
126.0	0.052	0.007	10.	1.

b

θ_{CM}	$\sigma_{el}(\theta)/$ σ_R	$\Delta\big(\sigma_{el}(\theta)/\sigma_R\big)$	$d\sigma_{in}/d\Omega$ (mb/sr)	$\Delta\big(d\sigma_{in}/d\Omega\big)$ (mb/sr)
12.9	1.10	0.02		
19.4	1.00	0.02		
29.0	1.02	0.03	225.	33.
40.1	0.99	0.02	285.	18.
49.5	0.88	0.03	250.	22.
58.8	0.79	0.03	191.	14.
66.4	0.77	0.03	191.	10.
70.9	0.79	0.03	166.	10.
73.8	0.89	0.03	170.	9.
76.8	0.78	0.03	158.	7.
82.0	0.74	0.09	77.	33.
86.0	0.59	0.05	99.	18.
90.0	0.44	0.03	85.	10.
96.0	0.21	0.02	56.	6.
102.0	0.08	0.02	25.	5.
114.0	0.030	0.009	5.	2.

inelastic scattering data [10]. We used the empirical potential of Wood-Saxon type expressed as

$$U_N(r) = -31.67 MeV fm^{-1} \frac{R_1 R_2}{R_1 + R_2}$$
$$\times \{1 + exp[(r - R_1 - R_2 - \Delta R)/a]\}^{-1},$$

where $R_i = 1.233 A_i^{1/3} - 0.98 A_i^{-1/3}$ fm and $a = 0.63$ fm. ΔR was adjusted in order to improve the fits. We used the same geometry for the imaginary part and adjusted the strength W. It should be mentioned that the computer code CCFUS [11], which is successfully used for the CC
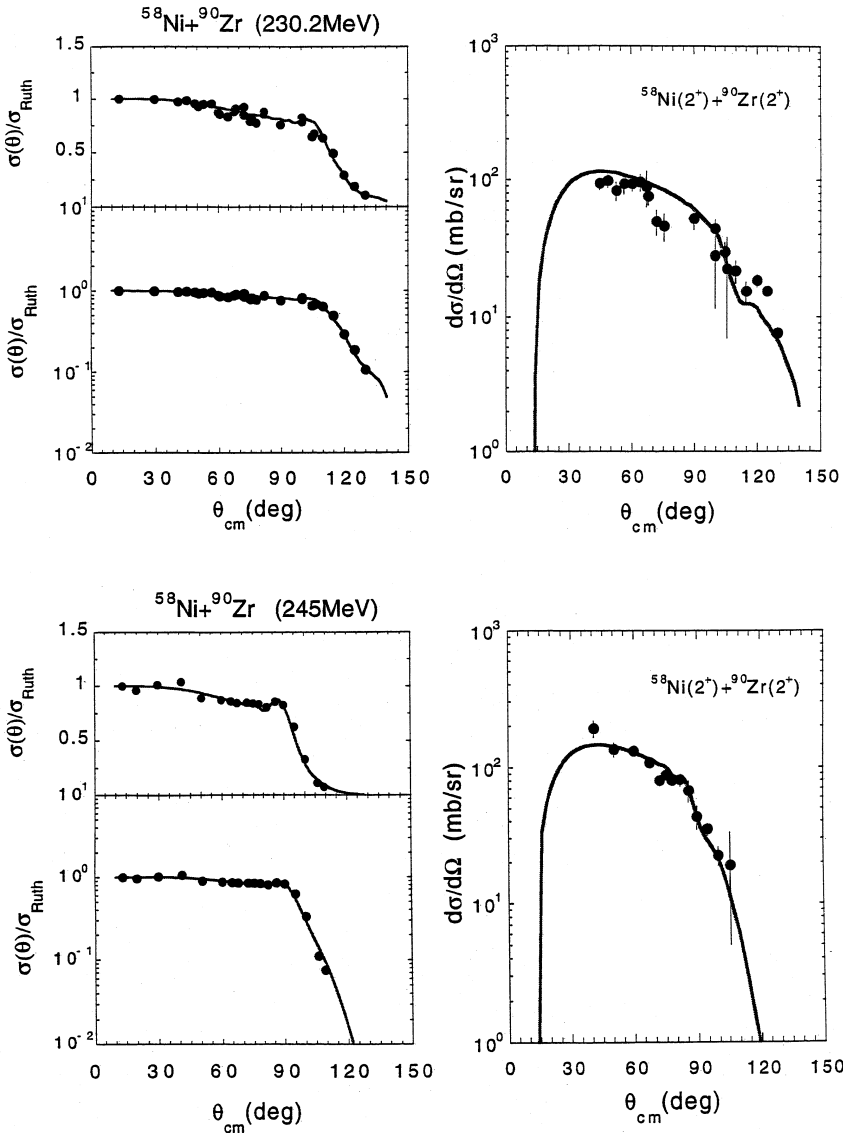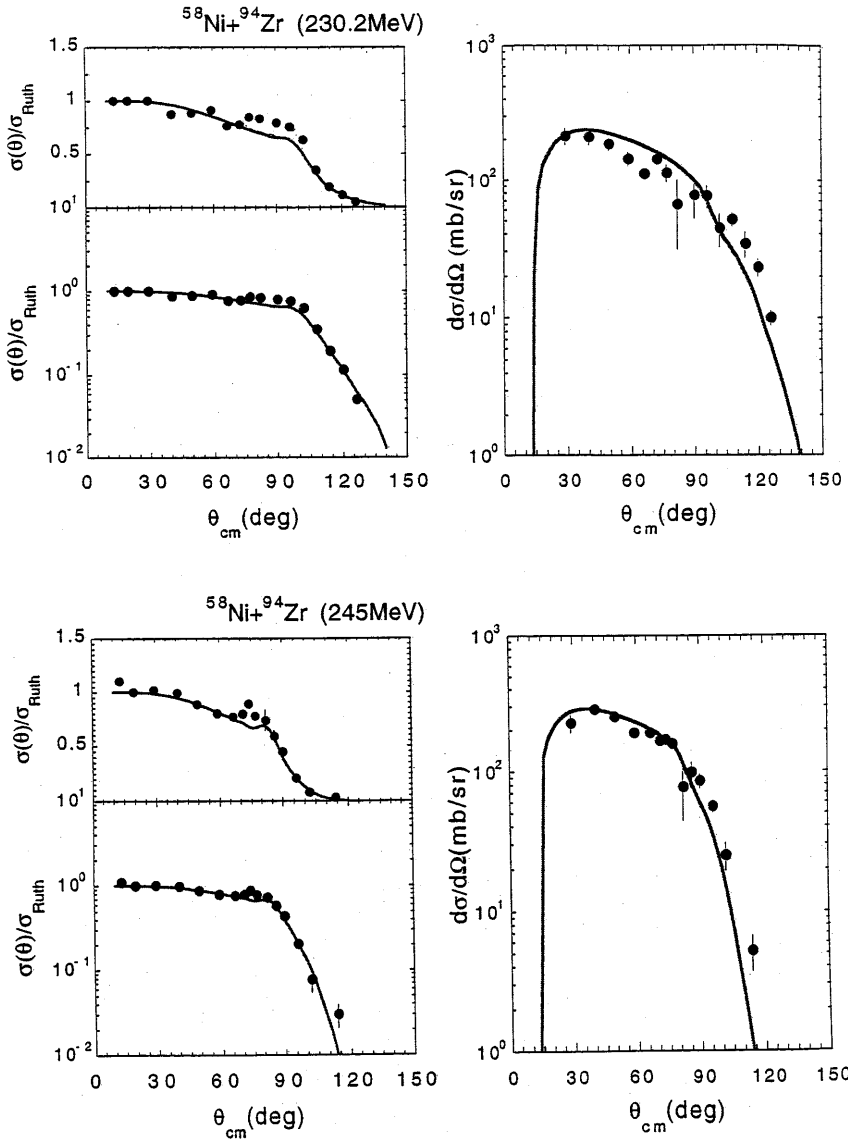
Fig. 3. Angular distributions for elastic and inelastic scattering at $E_{lab} = 230.2$ and 245.0 MeV for the ^{58}Ni + ^{90}Zr system. The solid lines are the results of the calculations. The left panels show elastic scattering angular distributions both in linear and in log scale. The right panels show the inelastic excitation to the 2^+ of ^{58}Ni and ^{90}Zr. The calculations have been performed assuming the same deformation parameters for the nuclear and Coulomb interaction with $\beta = 0.18$ for the ^{58}Ni(2^+) and with $\beta = 0.083$ for the ^{90}Zr(2^+)

analysis to fusion data, employs the same empirical real potential. The fusion cross sections for these systems were also analyzed [5] with the code CCFUS. Our elastic scattering data shows that the coupling to Coulomb excitation of surface vibrations plays important roles at forward angles around $\theta_{cm} \approx 60°$, since the cross section is clearly reduced compared with the Rutherford one. This reduction can not be reproduced by standard Optical Model calculations. The total cross sections for fusion evaporation processes, transfer reactions and deep inelastic scattering were measured at the same energies in a previous experiment [5]. In the present one we obtained the total inelastic scattering cross section. All these results are summarized in Table 3. We notice that inelastic scattering is the most dominant reaction channel. Therefore we took into account couplings to inelastic excitations of the collective states as the most dominant reaction channels in the CC analysis. Hence, the imaginary part of the nuclear interaction we are thus obtaining, has to be interpreted as

describing the depopulation of the entrance channel due to the channels that have not been explicitly included. In Fig. 5 we show the low energy level schemes of projectile and targets and the transitions included in the calculations are indicated by vertical arrows. The deformation parameters of the collective states of Ni and Zr have been extracted from the compilation of [12] and are listed in the captions of Figs. 3 and 6.

We used the computer code PTOLEMY [13] for the CC calculations. For the ^{90}Zr case a nuclear potential with $\Delta R = 0.28 fm$ and $W_0 = -15$ MeV was obtained at both incident energies by a best-fit procedure starting from the real empirical potential of [10], keeping for the imaginary part the same geometry and searching for ΔR and W_0. The angular distribution for inelastic scattering is reproduced well with the energy-independent optical potential. The obtained angular distributions at the two energies are shown with solid lines in Fig. 3. To stress the good fit to the data we also display the elastic scattering angular dis-

Fig. 4. The same as Fig. 3 but for the ^{58}Ni + ^{94}Zr system. In this case the inelastic angular distributions (right-hand side) get contributions from all the states up to an excitation energy of $\simeq 2$ MeV. For more details see caption to Fig. 6 below

Table 3. Angle and energy integrated cross sections(mb) obtained from the present and the previous measurements. The sum includes the inelastic, fusion-evapolation, transfer and deep-inelastic cross sections. The total rection cross sections σ_R obtained from the CC calculation is listed in the last column

Target	E_{lab} (MeV)	Inelastic	Fusion-evapolation [5]	Transfer [5]	Deep-inelastic [5]	Sum	σ_R
^{90}Zr	230.2	641.3±49.7	115.2±17.6	120.1±87.1	59.4±39.5	936.5±109.2	1042.7
	245.0	777.8±44.1	178.1±22.1	180.0±10.4	290.2±83.6	1426.1±97.6	1352.3
^{94}Zr	230.2	1097.5±58.0	189.6±28.8	285.9±49.6	109.7±61 .5	1682.7±102.2	1780.3
	245.0	1227.7±46.4	194.4±27.0	447.5±150.7	422.2±131.8	2291 .8±207.9	2097.1

tribution in a linear scale. It should be mentioned that our inelastic scattering data are reproduced well by using a deformed optical model potential, since the transitions are dominated by Coulomb potential at these incident energies.

We followed the same procedure for ^{94}Zr. The real part of the nuclear potential turns out to be the same while we had to use a stronger absorption ($W_0 = -25$ MeV) in

agreement with observation that the fusion, deep-inelastic and transfer cross sections are much larger in ^{94}Zr than in ^{90}Zr. The results of the calculations for the two energies are shown in Fig. 4 with solid lines. The experimental data are well reproduced by the energy-independent optical potential also for ^{58}Ni + ^{94}Zr . The right-hand side of Fig. 4 shows our results for the inclusive inelastic cross section, where we have summed the calculated cross section for
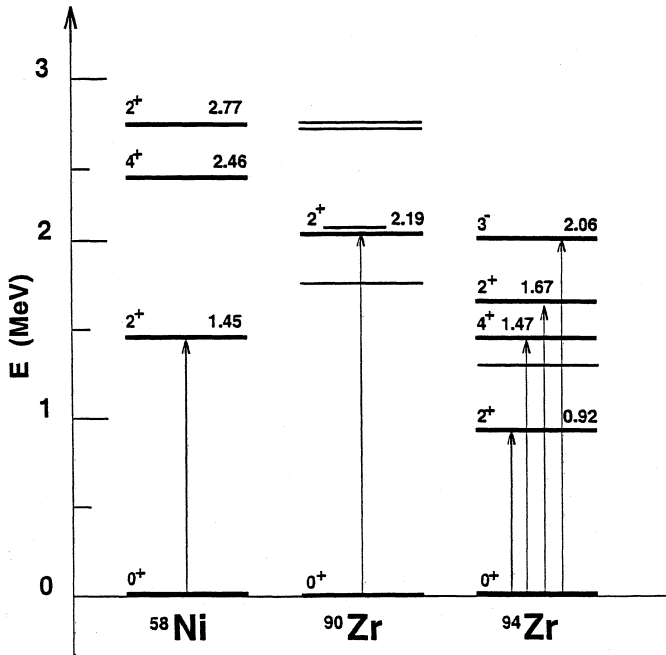
Fig. 5. Schematic representation of the excitation energy level schemes of ^{58}Ni, ^{90}Zr and ^{94}Zr to show the different transitions (vertical arrows) included in our calculations. The reorientation terms are not included in the figure but we have checked that their influences in the calculation are negligible

the 2^+ of ^{58}Ni and the first two 2^+ and 4^+ states of ^{94}Zr. In Fig. 6 we show the different calculated contributions to the total inelastic cross section.

The present results indicate that couplings to the inelastic excitations of both projectile and targets are sufficient to reproduce elastic and inelastic data with an energy-independent optical potential. Total reaction cross

sections σ_R were obtained from the present CC calculations with the code Ptolemy. Then we compared σ_R with the sum of the measured fusion, deep-inelastic, transfer reaction and inelastic scattering yields in Table 3. σ_R coincides with the sum of the measured cross sections within error bars. Therefore the imaginary part of the optical potential describes well the depopulation of the entrance channels due to fusion, transfer and deep inelastic channels that have not been explicitly included in the CC calculations.

4 Conclusion

We have reported here of pure elastic and inelastic scattering measurements of the systems ^{58}Ni + ^{90,94}Zr at two energies near the Coulomb barrier in order to obtain a unified description of ion-ion potentials. Angular distributions over a wide range of angles have been obtained. For these systems fusion, deep-inelastic and transfer cross sections had already been measured at the same energies in a previous experiment [5]. The present data have been analyzed in the coupled channels approach including the low-lying excitations of both projectile and targets which are the most dominant reaction channels. We have used the semi-empirical potential [9] which has been derived in terms of a folding potential, and which has been successfully used in the CC analysis of many sets of elastic scattering and fusion data. The agreement between experiment and theory is rather good using a nuclear real potential which is essentially target- and energy- independent. However, a stronger absorption is required for ^{58}Ni + ^{94}Zr than for ^{58}Ni + ^{90}Zr, in agreement of observation that the reaction cross section is much larger in the first system than in the second one. The total reaction cross section has been obtained by the CC calculation and has been compared with the sum of the measured cross sec-
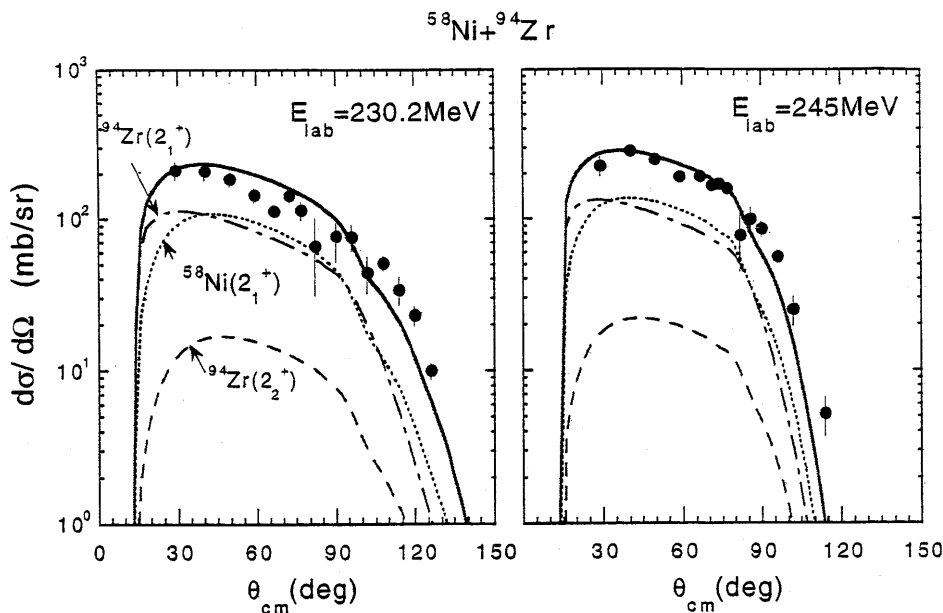
Fig. 6. Angular distributions for inelastic scattering of ^{58}Ni + ^{94}Zr at E_{lab} = 230.2 and 245.0 MeV where we show the different contributions to the inclusive cross section. The deformation parameters for the ^{94}Zr states are $\beta(2^+, 0.92$ MeV$)$= 0.095, $\beta(4^+, 1.45$ MeV$)$= 0.065, $\beta(2^+, 1.67$ MeV$)$= 0.06 and $\beta(3^-, 2.06$ MeV$)$= 0.14. Not shown are the contributions from the 4^+ and 3^- states in ^{94}Zr, since they are negligible

tions of the quasi-elastic, fusion and deep-inelastic processes. The agreement is good within the experimental errors. Therefore the CC calculation including both projectile and target inelastic excitations gives a good account not only of the elastic and inelastic scattering angular distributions but also of the cross sections for other types of reactions. The present results support the idea that the semi-empirical bare potential of the semi-empirical formula [9] is a good approximation to a unified ion-ion potential.

References

1. *Proceeding of the International Conference on Nuclear Structure and Heavy-Ion Reaction Dynamics, University of Notre Dame, Indiana 1990*, edited by R. Betts and J.J. Kolata. (Inst. of Phys. Conf. Series N 109, IOP Publ. Ltd., Bristol UK, 1991)

2. *Proceedings of the Workshop on Heavy Ion Collision at Energies near the Coulomb Barrier, Daresbury Laboratory, England, 1990*, edited by M.A. Nagarajan (Inst. of Phys. Conf. Series N 110, IOP Publ. Ltd., Bristol UK, 1991)

3. Y.Sugiyama, Y.Tomita, H.Ikezoe, K.Ideno, H.Fujita, T.Sugimitsu, N.Kato, S.Kubono and S.Landowne, Phy. Rev Lett. **62**, 1727 (1989)

4. A.M.Stefanini, G.Fortuna, A.Tivelli, W.Meczynski, S.Beghini, C.Signorini, S.Lunardi, M.Morando, Phy. Rev. Lett. **30**, 2088 (1984)

5. F. Scarlassara, S. Beghini, F. Soramel, C. Signorini, L. Corradi, G. Montagnoli, D.R. Napoli, A.M. Stefanini and Zhi-Chang Li, Z. Phys. A **338**, 171 (1991)

6. Y. Sugiyama,Y.Tomita, H.Ikezoe, E.Takekoshi, K.Ideno and N.Shikazono, Nucl. Instr. and Meth. **A281**, 512 (1989)

7. E. Takekoshi, Y. Sugiyama, H. Ikezoe, Y. Tomita, N. Shikazono, M. Sawada, K. Nagano and T. Tachikawa, Nucl. Instr. and Meth. **A237**, 512 (1985)

8. R.O. Sayer, Rev. de Phys. Appl. **12**, 1543 (1977)

9. R.A. Broglia and A. Winther, *Heavy-ion Reactions*, Vol 1, (Benjamine, New York, 1981)

10. H.Esbensen and F.Videbaek, Phy. Rev. **C40**, 126 (1989)

11. C.H.Dasso and S.Landowne,Comput. Phys. Commun. **46**, 187 (1987)

12. S. Raman, C.H. Malarkey, W.T. Milner, C.W. Nestor, JR. and P.H. Stelson, Atomic Data and Nuclear Data Tables **36**, 1 (1987)

13. M.J.Rhoades-Brown, M.H.Macfarlane and S.C.Pieper, Phys. Rev. **C21**, 2417, 2436 (1980)